International Journal of Scientific Reports
Sarhan NR et al. Int J Sci Rep. 2018 Jun;4(6):124-141
http://www.sci-rep.com
pISSN 2454-2156 | eISSN 2454-2164

DOI: http://dx.doi.org/10.18203/issn.2454-2156.IntJSciRep20182083

Original Research Article

Oxidative stress/PERK/apoptotic pathways interaction contribute to tramadol neurotoxicity in rat cerebral and cerebellar cortex and thyme enhances the antioxidant defense system: histological, immunohistochemical and ultrastructural study

Nahla Reda Sarhan[1]*, Yasmeen Mohamed Taalab[2]

[1]Department of Histology and Cell Biology, [2]Department of Forensic and Clinical Toxicology, Faculty of Medicine, Mansoura University, Egypt

Received: 01 May 2018
Revised: 16 May 2018
Accepted: 17 May 2018

***Correspondence:**
Dr. Nahla Reda Sarhan,
E-mail: nahlamohamedreda@yahoo.com

ABSTRACT

Background: Tramadol is an opioid analgesic with several adverse reactions. Oxidative and endoplasmic reticulum (ER) stresses have been involved in the molecular mechanisms underlying tramadol neurotoxicity. Importantly, protein kinase RNA-like ER kinase (PERK) is a key ER-downstream pathway that mediates apoptosis. We aimed to determine the cellular stresses interaction that mediates PERK-induced apoptosis in tramadol-treated rats and to assess the effect of thyme in enhancing the antioxidant defense system in the face of such stresses.
Methods: Forty male Sprague Dawley rats were randomized into 4 groups. Control group, thyme group received thyme extract (500 mg/kg/day) orally. Tramadol group received tramadol HCL (40 mg/Kg/day) dissolved in saline orally. Tramadol + Thyme group received tramadol and thyme extract. After 30 days, frontal motor and cerebellar cortex specimens were biochemically assessed for oxidative stress biomarkers and evaluated for histological, ultrastructural and immunohistochemical changes.
Results: Tramadol group showed a significant elevation in malondialdehyde level with a reduction in superoxide dismutase and catalase enzyme activities. Histologically and ultrastructurally, there were remarkable degenerative and apoptotic changes in the neurons and glial cells. In parallel, we detected a significant increase in integrated density for PERK immunostaining and number of caspase-3 positive cells/HPF compared to control. Tramadol + Thyme group showed improvement in oxidative stress parameters, histological and ultrastructural changes. Moreover, integrated density for PERK immunostaining and number of caspase-3 positive cells/HPF were significantly lower than Tramadol group.
Conclusions: Oxidative and ER stress-mediated PERK/apoptosis axis corroborates to the tramadol-induced neurotoxicity. Therapeutic strategies enhancing antioxidant activity and/or blocking ROS-mediated ER stress pathway may resolve tramadol neurotoxicity.

Keywords: Tramadol, Neurotoxicity, ER stress, Oxidative stress, PERK, Apoptosis

INTRODUCTION

Tramadol is a centrally acting synthetic opioid that acts through a non-classical pathway combining μ-opioid receptors activation and monoamines reuptake inhibition, resulting in blockade of nociceptive impulses at the nerve terminals.[1,2] This dual action promotes an enhanced analgesia with a low incidence of side effects.[2]

Although tramadol has been well-described for its better compliance and enhanced tolerability, its detrimental effect is yet a matter of concern. Tramadol has many adverse reactions including respiratory depression, convulsions, serotonin syndrome and fatal intoxication.[3] Oxidative stress, mitochondrial dysfunction, apoptosis, endoplasmic reticulum stress (ER-stress) and neurogenesis inhibition are the most common mechanisms of neurotoxicity following abusing drugs.[1] However, the exact mechanism is not completely understood.

The ER is an organelle responsible for balanced protein homeostasis via numerous cellular functions.[4] It organizes protein folding and degradation that get rid of the unfolded/misfolded proteins.[5]

Disturbance in ER homeostasis will result in ER stress with accumulation of unfolded/misfolded proteins inside its lumen. The presence of these abnormal proteins within the ER activates series of adaptive cellular response namely, the unfolded protein response (UPR), to restore ER normal functions via prosurvival and proapoptotic mechanisms.[6,7] Three major ER transmembrane sensing proteins have been recognized as the main signaling pathways of UPR; protein kinase RNA-like ER kinase (PERK), inositol-requiring enzyme 1 (IRE1), and activating transcription factor 6 (ATF6).[8] Upon cellular stress caused by a wide range of internal stresses and environmental exposure such as oxidative stress, toxic agent/drug and radiation, these kinases will be activated.[4,7,9]

Over the past decade, several studies link ER and oxidative stress in multiple physiological and pathophysiological conditions. Excessive reactive oxygen species (ROS) initiates distress of cellular redox balance which result in apoptosis.[10-12] A model called ROS dependent ER stress have been concurrently explained to indicate the two stresses that are closely linked events in cellular homeostasis and apoptosis.[11,12] The molecular events coupling ROS and components of ER stress is yet to be fully elucidated. Meanwhile, changes in protein folding pathways produces an ROS imbalance, indirectly disturbing both ER and redox homeostasis and this response can be reversed by antioxidants like thyme vulgaris.[13,14] Thyme is a natural herb belongs to lamiacea family. It has antioxidant properties and free radical scavenger activity. Additionally, it has an anti-inflammatory effect.[14]

PERK as a major element of UPR might be the key player in tramadol-induced neurotoxicity via linking both oxidative and ER stress pathways. With the insufficient information regarding the molecular and biochemical mechanisms underlying tramadol toxicodynamic effects, studying its in *vivo* effects has become our research focus to investigate the role of oxidative and ER stress pathways through determination of biochemical, histological, and ultrastructural changes together with ER stress/apoptosis biomarkers expression in motor cerebral and cerebellar cortex of a rat model of tramadol toxicity. Further, to evaluate the effect of thyme extract in enhancing the antioxidant defense system in the face of cellular stress.

METHODS

Chemicals

Contramal (tramadol HCl): was provided as 100 mg tablets (Grunenthal, Italy).

Thyme aqueous extract: Thyme dry leaves were obtained from the local market. By an electrical chopper thyme leaves were crushed into fine powder. Then 100 gm of the powder was exposed to extraction with 200 ml of boiled distilled water (DW) in a covered flask for 30 minutes. The extract was cooled and filtered to remove any particulate material then the filtrate was left to dry in a vacuum. The required doses were weighed and reconstituted in 5 ml of DW immediately before administration.[15]

Animals and experimental protocol

The present study was performed on 40 male Sprague Dawley rats weighing between 180-200 g. The animals were obtained from Mansoura Experimental Research Center (MERC) and used according to the Guidelines for Care and Use of laboratory animals. The animals were kept in separate cages with average temperature (22-24 C°) and humidity in an adequately ventilated room under a regular 12h light/12h dark cycle and were allowed free access to food and water ad libitum. The experimental protocol was approved by the Institutional Review Board of Faculty of Medicine, Mansoura University (Code Number: R/17.11.32).

The animals were randomly allocated into 4 groups (10 rats each): Control group received 1 ml of normal saline 0.9% orally by oro-gastric tube. Thyme group: received thyme extract in a dose of 500 mg/kg/day orally through oro-gastric tube.[15] Tramadol group: treated with oral dose of tramadol HCL (40 mg/Kg/day) suspended in saline solution through oro-gastric tube.[1,16] Tramadol + Thyme group treated with combined oral doses of tramadol HCL and thyme extract daily at the same doses and route of administration of Tramadol and Thyme groups.

Specimens acquisition

At the end of 30 days-experiment and 24-h after the last tramadol dose, the rats were anesthetized with sodium pentobarbital (40 mg/kg) intraperitoneal and perfused through the left ventricle with 0.1 M sodium phosphate buffer (pH 7.4) containing 2.5% glutaraldehyde. Then rats were sacrificed by decapitation. The skull vaults were removed and the intact brains were dissected out. Specimens from the frontal motor cortex and the

cerebellum were taken and processed for biochemical, light and electron microscopic studies.

Preparation of tissue homogenates for oxidative stress biochemical studies

The excised brain tissue samples were washed with phosphate buffered saline solution (pH 7.4) with 0.16 mg/ml heparin to remove red blood cells and clots. Then the tissue were homogenized in 5-10 ml cold buffer (50 mM potassium phosphate, pH 7.5) per gram tissue and centrifuged at 4000 r.p.m for 15 minutes at 4°C. The supernatant was used for the following biochemical assays:

Lipid peroxidation assay

Lipid peroxidation was estimated colorimetrically by measuring malondialdehyde (MDA) level according to thiobarbituric acid (TBA) reaction described by Ohkawa et al.[17] The kit was provided by Bio-Diagnostics (Dokki, Giza, Egypt, catalog number. MD 2529). MDA content is expressed as nmol/ml.

Antioxidant enzymes activity assays

Superoxide dismutase (SOD) activity was determined according to the procedure described by Nishikimi et al and expressed as U/ml. Catalase (CAT) activity was determined according to the method of Aebi, and expressed as U/L.[18,19] Enzyme activities were measured using colorimetric kits (Bio-Diagnostics; Dokki, Giza, Egypt, catalog number; SD 2521, CA 2517) for SOD and CAT respectively.

Light microscopic study

Small pieces from the frontal motor cortex and cerebellum were fixed in 10% neutral buffered formalin for 24 hour, dehydrated in ascending grades of alcohol, cleared in xylene and embedded in paraffin wax. Serial paraffin sections (5 µm) were cut and prepared for the following histological and immunohistochemical staining:

Hematoxylin and eosin (H&E) staining was done for general histological examination and detection of any structural changes.[20]

Immunohistochemical staining

Immunohistochemical staining was carried out using Avidin–Biotin–Peroxidase technique.[21] Paraffin tissue sections were stained with anti-PERK rabbit polyclonal antibody (Boster Bio Co, catalog no A01992-1, Pleasanton, CA; diluted 1/100) as a marker for ER stress and with anti-caspase-3 rabbit polyclonal antibody (Diagnostic Biosystems, catalog no RP096, USA diluted 1/100) for detection of apoptosis. Negative controls were done with the same technique but without incubating the sections with the primary antibodies. Human gastric mucosa and palatine tonsil were used as positive control slides for PERK and activated caspase-3 respectively. Brown cytoplasmic staining was considered as positive reaction.

Electron microscopic study

Very small pieces of the frontal motor cortex and cerebellum 1x1 mm in size were fixed in 2.5% buffered glutaraldehyde, and then processed to obtain semithin and ultrathin sections. Ultrathin sections (60–80 nm) were cut, stained with uranyl acetate and lead citrate and examined by JEOL-JEM-100 SX transmission electron microscope in Electron Microscopy unit, Faculty of Agriculture, Mansoura University, Egypt.[22]

Quantitative assessment of immunostained sections

Integrated density (ID) of PERK immunostaining and the number of caspase-3 positive cells/high power field (HPF) in the outer and inner pyramidal layers of frontal motor cortex and the three layers of cerebellar cortex were evaluated from PERK and caspase-3 immunostained sections respectively. For the assessment of these morphometric parameters, 10 non-overlapping microscopic fields from each animal in all groups were photographed by an Olympus digital camera (E420, China) installed on Olympus microscope with 0.5x photo adaptor at x400 magnification. The images were then analyzed on Intel Core 13 based computer using VideoTesT Morphology software (VideoTesT, Russia, Saint-Petersburg).

Statistical analysis

The Data were analyzed using Statistical software (SPSS V23, Inc., IL, USA). For statistical comparison between different groups; one way analysis of variance (ANOVA) test followed by post-hoc Tukey test were used for comparing quantitative parametric data while Kruskal-Wallis test followed by Dunn's test were used for comparing quantitative non-parametric data. Quantitative parametric data were represented as mean±standard deviation, while quantitative non-parametric data were presented in median and interquartile range (IQR). $P<0.05$ was considered statistically significant.

RESULTS

Biochemical findings

MDA level

No Statistically significant difference was found in MDA level in the cerebral and cerebellar cortex between the thyme group and control group. The Tramadol group showed a significant elevation ($p<0.05$) in MDA level as compared to Control group. On the other hand, MDA level decreased significantly ($p<0.05$) in Tramadol+ Thyme group as compared to tramadol group but showed significant increase compared to control group (Table 1).

Table 1: MDA level (nmol/ml) among the studied groups.

		Control	Thyme gp	Tramadol gp	Tramadol+Thyme gp	ANOVA P value
Cerebral Cortex	Mean	1.32	1.36	6.38[ab]	3.10 [abc]	<0.001*
	±SD	0.16	0.20	2.56	1.07	
Cerebellum	Mean	1.26	1.36	6.28 [ab]	3.50 [abc]	
	±SD	0.11	0.15	2.62	1.38	<0.001*

SD: standard deviation; P:Probability*:significance <0.05; Test used: One way ANOVA followed by post-hoc tukey; a: significance relative to Control Group; b: significance relative to Thyme Group; c: significance relative to Tramadol Group.

Table 2: SOD and CAT activities among the studied groups.

			Control	Thyme gp	Tramadol gp	Tramadol +Thyme gp	ANOVA P value
Cerebral cortex	SOD (U/ml)	Mean	21.83	22.43	10.17 [ab]	16.27 [abc]	< 0.001*
		±SD	0.13	1.13	0.04	1.65	
	CAT (U/L)	Mean	0.297	0.292	0.236 [ab]	0.271 [abc]	< 0.001*
		±SD	0.002	0.009	0.012	0.006	
Cerebellum	SOD (U/ml)	Mean	21.41	22.21	11.71 [ab]	15.13 [abc]	< 0.001*
		±SD	0.29	1.10	0.13	2.39	
	CAT (U/L)	Mean	0.342	0.34	0.289 [ab]	0.312 [abc]	<0.001*
		±SD	0.003	0.015	0.004	0.002	

SD: standard deviation; P: Probability*: significance < 0.05; Test used: One way ANOVA followed by post-hoc tukey; a: significance relative to Control Group; b: significance relative to Thyme Group; c: significance relative to Tramadol Group.

Table 3: Integrated density (ID) of PERK immunostaining among the studied groups.

ID*10^4		Control	Thyme gp	Tramadol gp	Tramadol +Thyme gp	ANOVA P value
Cerebral cortex	Mean	64.68	74.61	1708.6[ab]	566.3[abc]	< 0.001*
	±SD	3.23	3.73	85.4	28.31	
Cerebellum	Mean	31.2	28.72	1410.4[ab]	652.2[abc]	< 0.001*
	±SD	1.56	1.43	70.49	32.6	

SD: standard deviation; P: Probability*: significance < 0.05; Test used: One way ANOVA followed by post-hoc tukey; a: significance relative to Control Group; b: significance relative to Thyme Group; c: significance relative to Tramadol Group.

Table 4: Number of Caspase-3 positive cells / HPF among the studied groups.

		Control	Thyme gp	Tramadol gp	Tramadol+Thyme gp	Kruskal- Wallis P value
Cerebral Cortex	Median	0.00	0.00	10.00 [ab]	4.00 [abc]	<0.001*
	IQR	0.00-0.00	0.00-.00	7.00-12.00	4.00-4.00	
Cerebellum	Median	0.00	0.00	12.00 [ab]	4.00 [abc]	<0.001*
	IQR	0.00-0.00	0.00-1.00	10.00-15.00	3.00-5.00	

IQR: interquartile range; P:Probability*: significance <0.05; Test used: Kruskal- wallis followed by post-hoc Dunn's test; a: significance relative to Control Group; b: significance relative to Thyme Group; c: significance relative to Tramadol Group.

SOD and CAT activities

SOD and CAT activities in the cerebral and cerebellar cortex showed no statistically significant changes in Thyme group as compared to Control group. However, Tramadol group showed a significant reduction ($p<0.05$) in CAT and SOD activities as compared to the Control group. On the other hand, the activities of CAT and SOD increased significantly ($p<0.05$) in Tramadol + Thyme group as compared to tramadol group however they still significantly lower than the control group (Table 2).

Histological and immunohistochemical findings

Cerebral cortex

Examination of H &E stained sections of the frontal motor cortex of the Control and Thyme groups were similar and demonstrated the normal histological structure. Six cortical layers were identified from outside inwards: molecular, outer granular, outer pyramidal, inner granular, inner pyramidal and multiform layer (Figure 1A). The main cellular populations of these layers are the pyramidal neurons, the granular neurons and the neuroglial cells. The cells were scattered in an

eosinophilic neuropil that formed of neuronal and glial cell processes. The inner pyramidal layer (IPL) was selected as it contains medium and large sized pyramidal cells and granular cells. The pyramidal cells revealed large vesicular nuclei, basophilic cytoplasm and long apical dendrites and the granular cells were rounded with large rounded vesicular nuclei. While the neuroglial cells were smaller and showed small dense nuclei (Figure 1B, C).

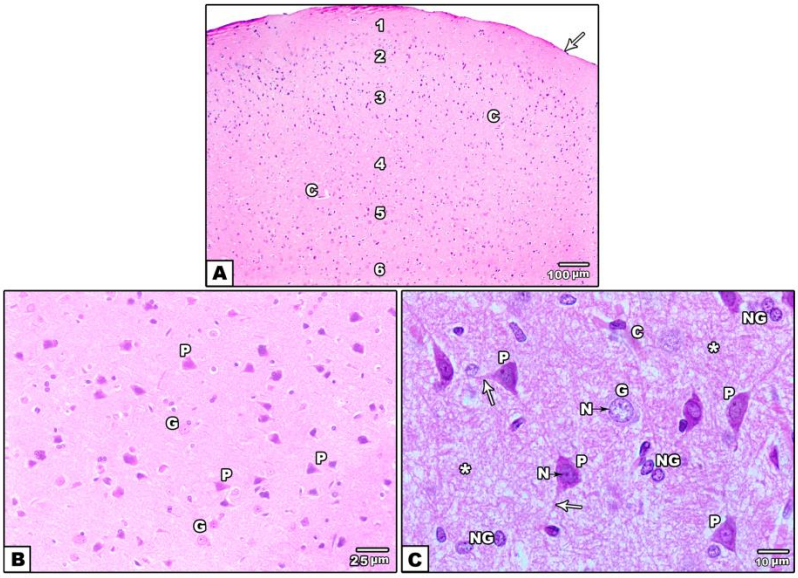

Figure 1: Photomicrographs of the frontal motor cerebral cortex of the Control group. (A) showing the six cortical layers that include the molecular (1), outer granular (2), outer pyramidal (3), inner granular (4), inner pyramidal (5), and multiform layer (6). Blood capillaries (C) are also seen. A layer of pia matter (arrow) covers the molecular layer is shown. (B and C) showing the inner pyramidal layer containing large pyramidal (P) and granular cells (G). The P cells have basophilic cytoplasm, large vesicular nuclei (N) and long apical dendrites (arrows) while G cells are rounded and show large rounded vesicular nuclei (N). Neuroglial cells (NG) with small dense nuclei are also found. The Neuropil (*) forms the background for the cells. A Blood capillary (C) is also observed (H&E; Ax100, Bx400; Cx1000).

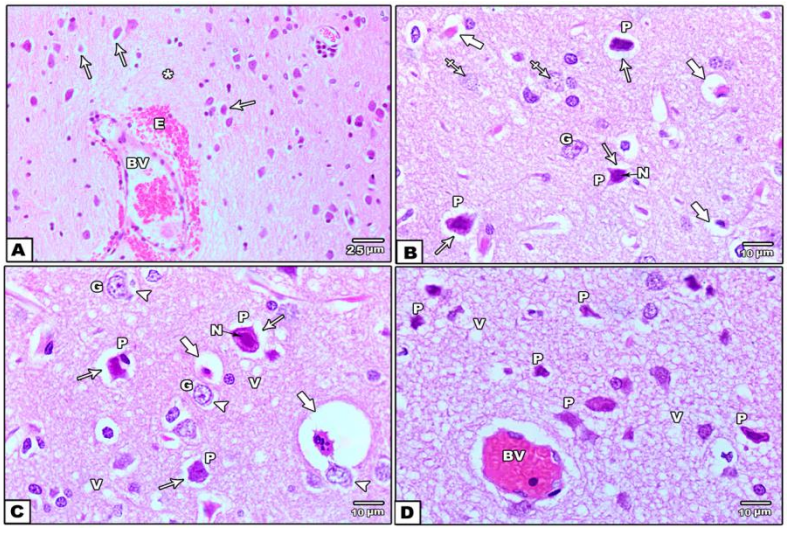

Figure 2: Photomicrographs of the frontal motor cerebral cortex of Tramadol group (inner pyramidal layer). (A) showing dilated congested blood vessels (BV) with extravasation (E) of blood into the neuropil (*). Some pyramidal cells surrounded by pericellular halos (arrows). (B and C) The pyramidal cells (P) are dark shrunken with darkly stained nuclei (N) and surrounded by pericellular halos (arrows). Some granular cells (G) are shrunken and have pericellular halos (arrow heads). Other G cells appear as ghosts without nucleoli and faintly stained (crossed arrows). Many apoptotic cells (thick arrows) that have little acidophilic cytoplasm, fragments of darkly stained nuclei and surrounded by clear halos are observed. Note vacuolization of the neuropil (V). (D): Most of the pyramidal cells (P) are markedly shrunken with darkly stained nuclei. Congestion of blood vessels (BV) and extreme vacuolation (V) of the neuropil are also noticed (H&E; Ax400, B-D x1000).

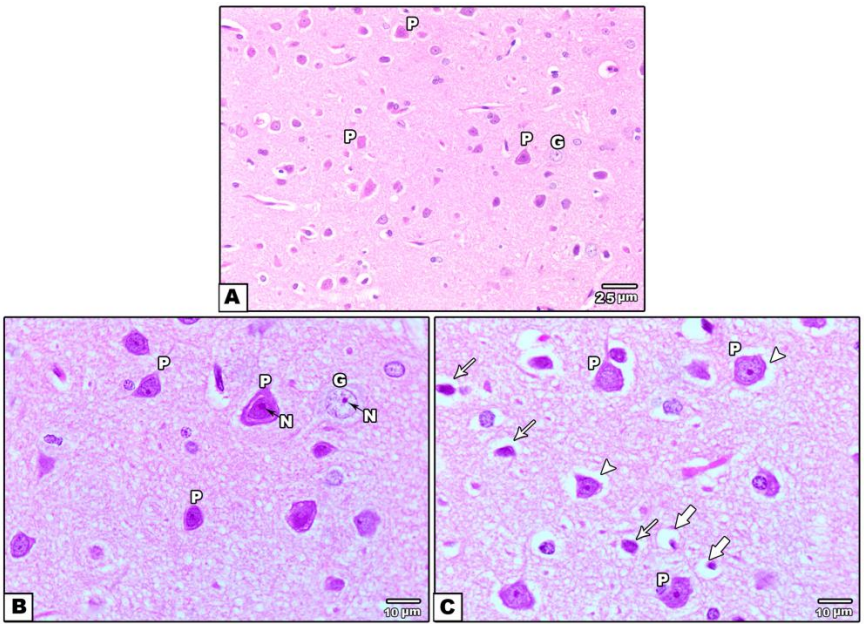

Figure 3: Photomicrographs of the frontal motor cerebral cortex of Tramadol+Thyme group (inner pyramidal layer). (A, B) (B: higher magnification of A), and (C) The majority of the pyramidal cells (P) and the granular cells (G) are intact with vesicular nuclei (N) and some of them surrounded by pericellular halos (arrow heads). However; some pyramidal cells appear shrunken and surrounded by halos (arrows). Also, few apoptotic cells (thick arrows) are noted (H&E; A x 400, B & C x1000)

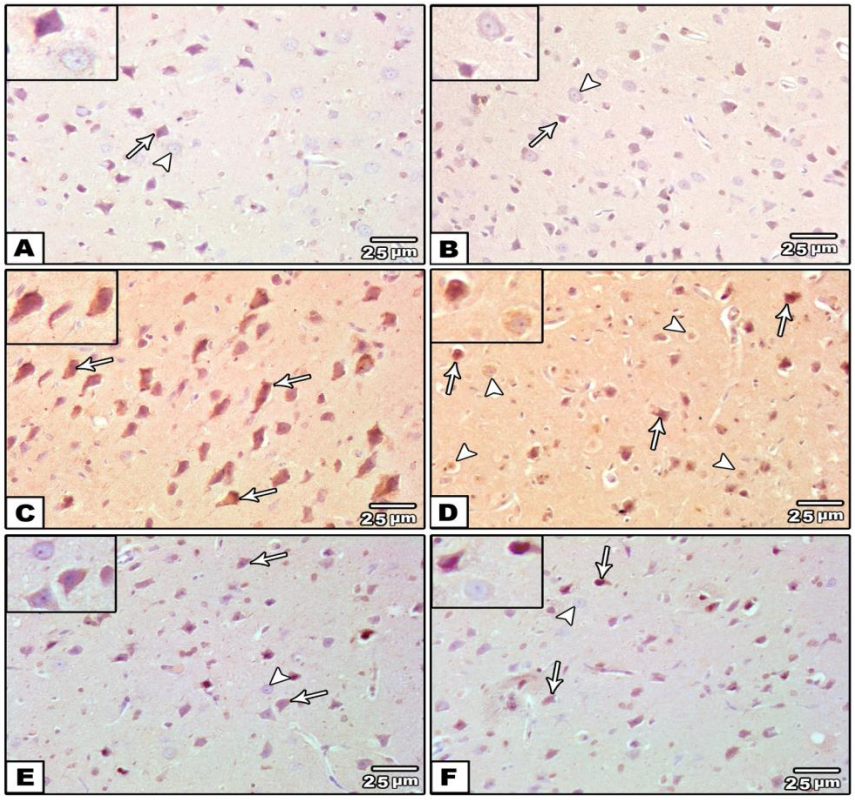

Figure 4: PERK expression in the frontal motor cortex of the studied groups. (A&B) the Control group showing weak positive cytoplasmic PERK immune reaction in the pyramidal cells (arrows) and granular cells (arrow heads). (C&D) Tramadol group showing strong positive PERK immune reaction in the pyramidal cells (arrows) and granular cells (arrow heads). (E&F) Tramadol + Thyme group showing weak to moderate positive PERK immune reaction in the pyramidal cells (arrows) and weak immune reaction in the granular cells (arrow heads) (Anti-PERK; x400, insets: high magnification x1000).

The Tramadol group showed multifocal histological alterations in the different cortical layers compared to control group. The pyramidal neurons were the most affected cell type. In the IPL; the majority of the pyramidal cells were dark shrunken, with densely stained nuclei and surrounded by pericellular halos. Some granular cells were shrunken and surrounded by pericellular halos. While other granular cells lost their nucleoli, faintly stained and appeared as ghosts. There were also numerous apoptotic cells had little acidophilic cytoplasm, fragmented darkly stained nuclei and surrounded by clear halos. Neuropil vacuolization and dilated congested blood vessels with blood extravasation into the surrounding neuropil were also noticed (Figure 2). In contrast, Tramadol + Thyme group showed improved histological appearance. Most of the pyramidal and granular cells were relatively intact. However, some shrunken pyramidal cells that surrounded by halos and few apoptotic cells were observed (Figure 3).

Immunohistochemically stained sections for PERK revealed weak positive immune reaction in the pyramidal cells and the granular cells of Control group frontal motor cortex (Figure 4 A, B). Thyme group showed the same pattern of PERK immune reaction and a non-significant difference in integrated density (ID) of PERK immunostaining in the pyramidal layers of motor cortex as compared to Control group (Table 3). However, in Tramadol group a strong positive PERK immune reaction was found in the pyramidal cells and the granular cells (Figure 4 C, D). On the other hand, Tramadol + Thyme group demonstrated a weak to moderate positive PERK immune reaction in the pyramidal cells and a weak immune reaction in the granular cells (Figure 4 E, F). The ID of PERK immunostaining showed a significant increase ($p<0.05$) in Tramadol group as compared to control group. However, it showed a significant decrease ($p<0.05$) in Tramadol + Thyme group as compared to Tramadol group but still significantly higher than Control group (Table 3).

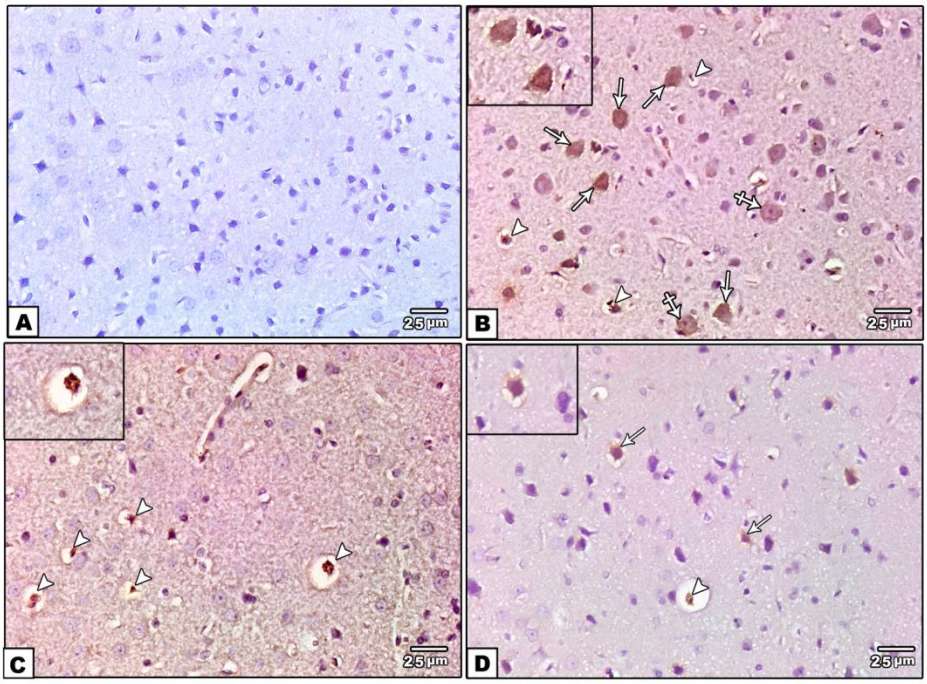

Figure 5: Caspase-3 immunostaining in the frontal motor cortex of the studied groups. (A) Control group showing caspase-3 negative immune reaction in the cells of cerebral cortex. (B&C) Tramadol group showing many caspase-3 positive pyramidal (arrows) and, granular cells (crossed arrows). Many caspase-3 positive apoptotic cells (arrow heads) were also observed. (D) Tramadol + Thyme group showing few caspase-3 positive pyramidal (arrows) and apoptotic cells (arrow heads) (anti-Caspase-3; x400, insets: high magnification x1000).

Immunohistochemical staining for Caspase-3 showed no caspase-3 positive cells in the Control group frontal motor cortex (Figure 5 A). Thyme group was similar to Control group in the immunoreactivity pattern and showed non-significant difference in the mean number of caspase-3 positive cells/HPF as compared to Control (Table 4). In Tramadol group, there were many caspase-3 positive pyramidal and granular cells. Many caspase-3 positive apoptotic cells were also noticed (Figure 5 B, C). However, in Tramadol + Thyme group few caspase-3 positive pyramidal and apoptotic cells were found (Figure 5 D). The number of caspase-3 positive cells/HPF was significantly higher ($p<0.05$) in Tramadol group as compared to Control group. While it was significantly lower ($p<0.05$) in Tramadol + Thyme group as compared to Tramadol group although it still higher than that observed in Control group (Table 4).

Cerebellar cortex

In H&E stained sections, the Control and Thyme groups showed the same normal histological structure of cerebellar cortex that was organized in three layers outer molecular, middle purkinje and inner granular layer. The molecular layer showed few scattered nuclei of stellate cells and basket cells. Purkinje layer showed large pyriform purkinje cells that arranged in one row and had rounded vesicular nuclei with prominent nucleoli. Perineural glial cells were seen around purkinje cells. The granular layer contained closely packed small granular cells with darkly stained nuclei and little cytoplasm and scattered Golgi cells with vesicular nuclei. Acidophilic cerebellar islands that consisted of synaptic complexes were also observed throughout this layer (Figure 6 A, B).

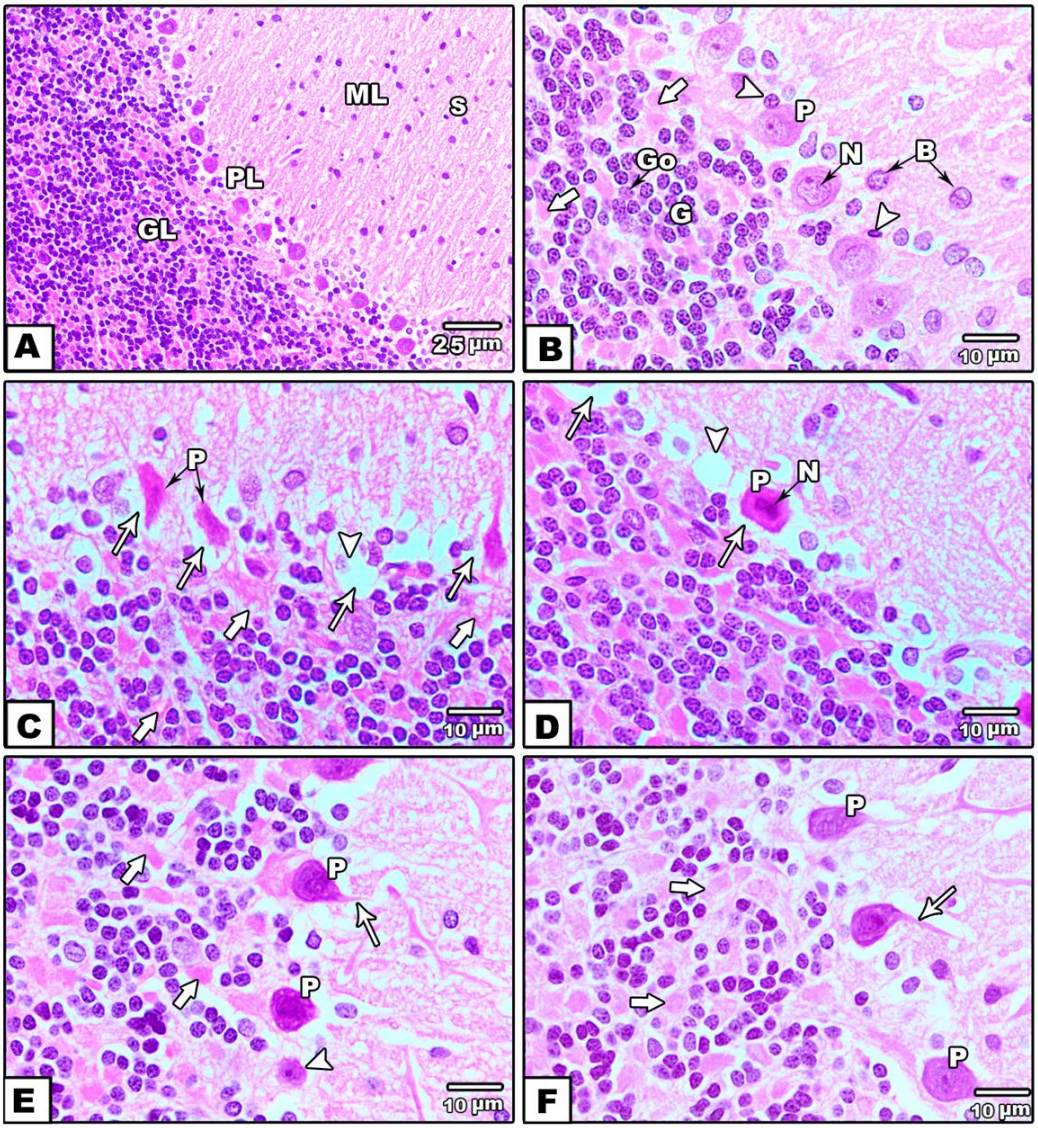

Figure 6: Photomicrographs of the cerebellar cortex of the studied groups. (A&B) the Control group showing the molecular layer (ML), purkinje layer (PL) and granular layer (GL) of the cerebellar cortex. The ML shows few scattered stellate cells (S) and basket cells (B). The PL contains large pyriform purkinje cells (P) with rounded vesicular nuclei (N). Perineural glial cells (arrow heads) are seen around P cells. The GL contains numerous small granular cells (G) with darkly stained nuclei, Golgi cells (Go) with vesicular nuclei and acidophilic cerebellar islands (thick arrows). (C&D) the Tramadol group showing few, deformed and shrunken purkinje cells (P) that surrounded by empty spaces (arrows) and have hardly detected nuclei or condensed shrunken nuclei (N). Vacuolations of the cerebellar islands (thick arrows) is also noted. Some empty areas with loss of P cells are also noticed (arrow heads) (E&F) the Tramadol + Thyme group showing relatively intact purkinje cells (P) that appear with vesicular nuclei. Note their apical dendrites (arrows). Few shrunken P cells (arrow head) were found in some areas. The cerebellar islands (thick arrows) appear intact (H&E; A x400, B-F x1000).

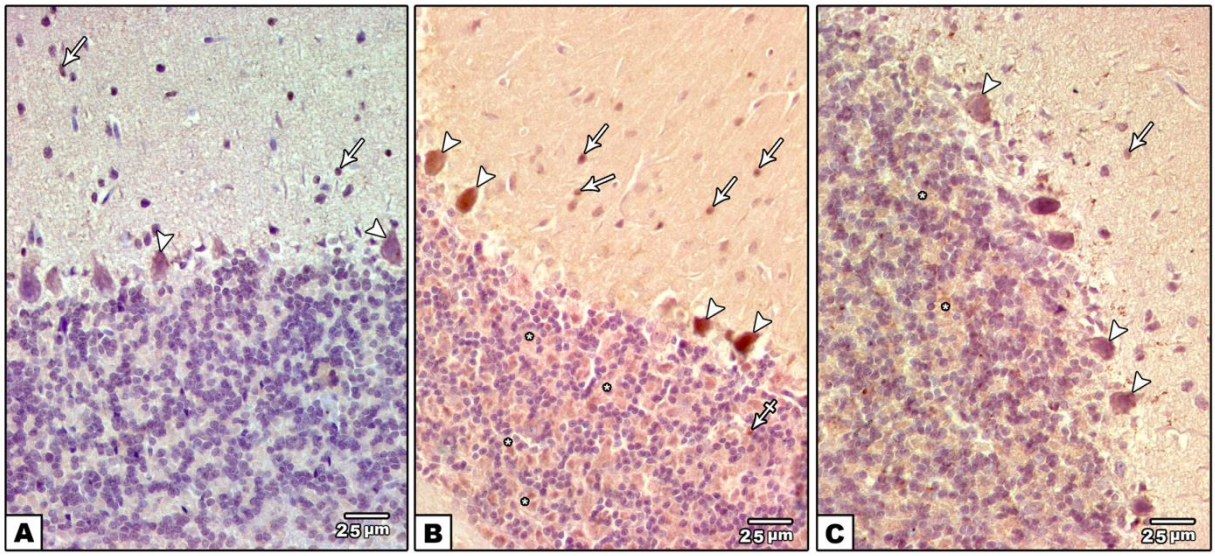

Figure 7: PERK expression in the cerebellar cortex of the different groups. (A) the Control group showing weak PERK immunostaining in some cells of the molecular layer (arrows) and some purkinje cells (arrow heads). (B) Tramadol group showing strong PERK immunostaining in some cells of molecular layer (arrows) and all purkinje cells (arrow heads). Some cells (crossed arrow) in the granular layer and the cerebellar islands (*) show moderate PERK immunostaining. (C) the Tramadol + thyme group showing weak to moderate PERK immunostaining in some cells of the molecular layer (arrow), in purkinje cells (arrow heads) and in cerebellar islands (*) (Anti-PERK; X400).

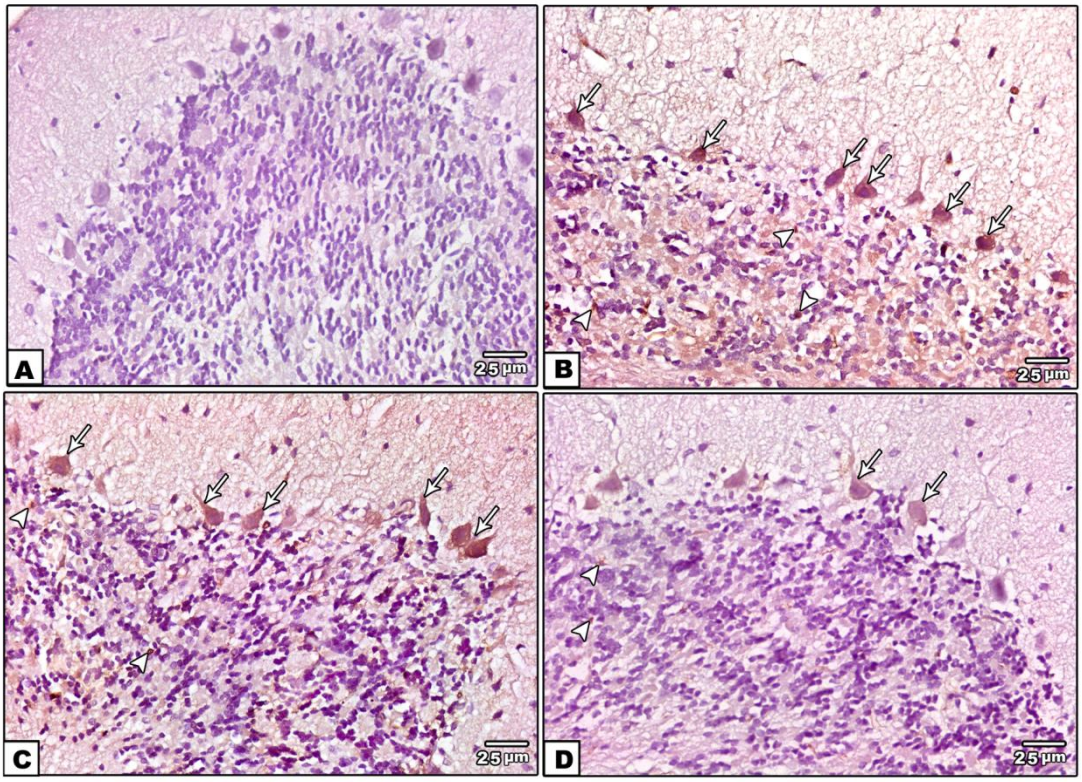

Figure 8: Caspase-3 immunostaining in the cerebellar cortex of the studied groups. (A) the Control group showing no caspase-3 positive cells in the cerebellar cortex. (B&C) Tramadol group showing strong positive caspase-3 immune reaction in many purkinje cells (arrows) and in some cells of the granular layer (arrow heads). (D) Tramadol + Thyme group showing caspase-3 weak to moderate immune reaction in few purkinje cells (arrows). Few caspase-3 positive cells are noted in the granular layer (arrow heads) (Anti-caspase-3; X 400).

In Tramadol group, histological changes were detected that were more evident in the purkinje layer. Purkinje cells were few in number, shrunken and deformed. They were surrounded by empty spaces and their nuclei were hardly detected or dense and shrunken. Vacuolations of the cerebellar islands were also observed (Figure 6 C, D).

Tramadol + Thyme group showed improvement with less histological changes as compared to Tramadol group. Most of purkinje cells were relatively intact with vesicular nuclei and the cerebellar islands showed normal structure. However, few shrunken purkinje cells and vacuolations of cerebellar islands were still found in some areas (Figure 6 E, F).

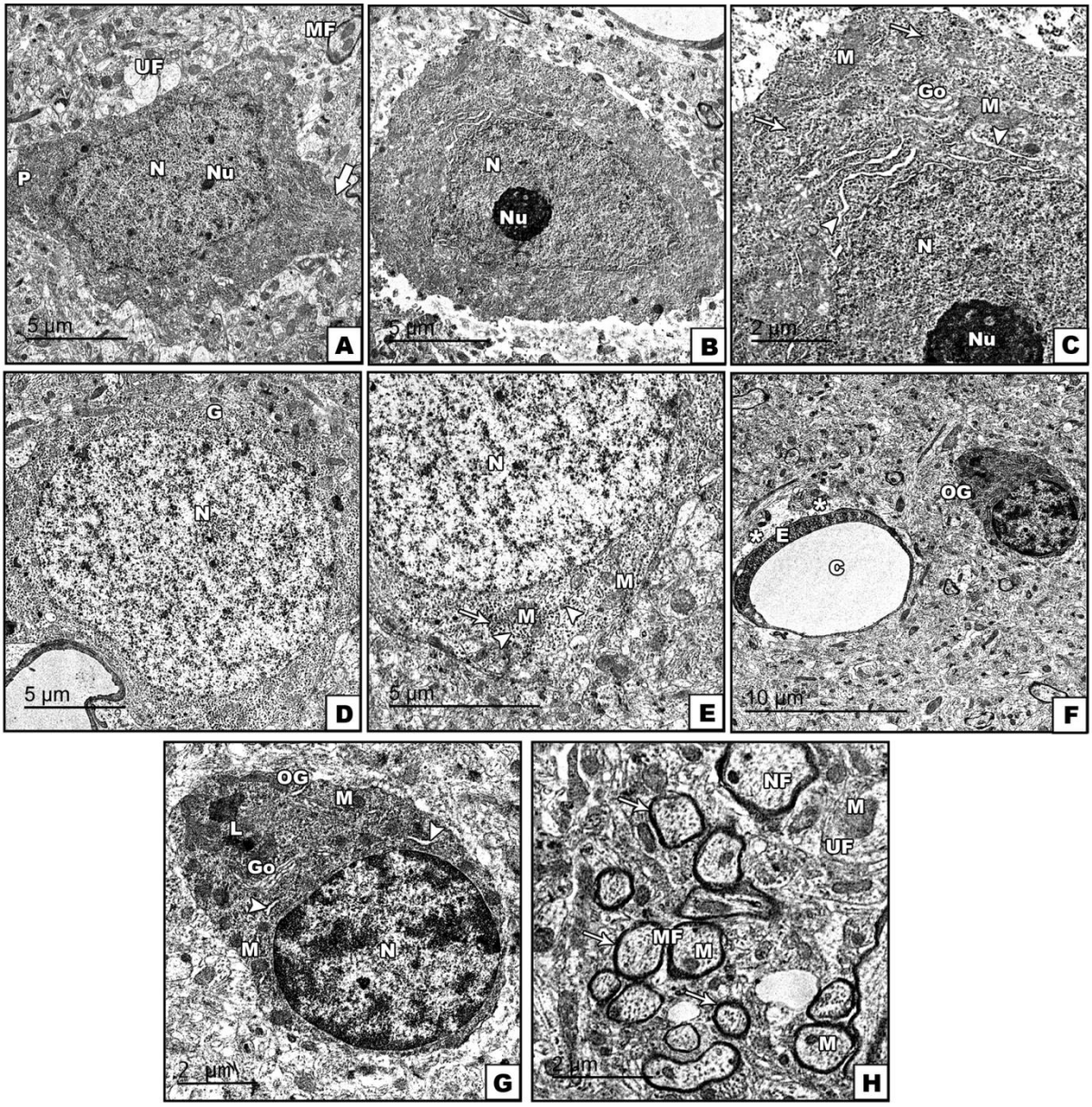

Figure 9: Electron micrographs of the motor cortex of the control group. (A, B & C) (C: high magnification of B): The pyramidal cell (P) showing vesicular nucleus (N) with prominent nucleolus (Nu). Golgi saccules (Go), Mitochondria (M), rER (arrow heads) and ribosomes (arrows) are seen in the cytoplasm. Note one of its apical dendrites (thick arrow), myelinated (MF) and unmyelinated nerve fibers (UF) in the surrounding neuropil (A&B x1000, C x2000) (D&E) (E: high magnification of D): showing a granular cell (G) containing rounded euchromatic nucleus (N), rER (arrow heads), mitochondria (M) and ribosomes (arrow) (D x1000, E x1500). (F and G) (G: high magnification of F): In the neuropil, an oligodendrocyte (OG) and a blood capillary (C) are seen. The OG shows heterochromatic nucleus (N), mitochondria (M), Golgi apparatus (Go), rER (arrow heads) and some lysosomes (L).The C is lined with endothelial cells (E) and surrounded by astrocytes end feet (*) (F x800, G x2000). (H) the myelinated (MF) and unmyelinated fibers (UF) show mitochondria (M) and neurofibrils (NF). Regularly arranged compact myelin lamellae (arrows) are observed in the MF (x2500).

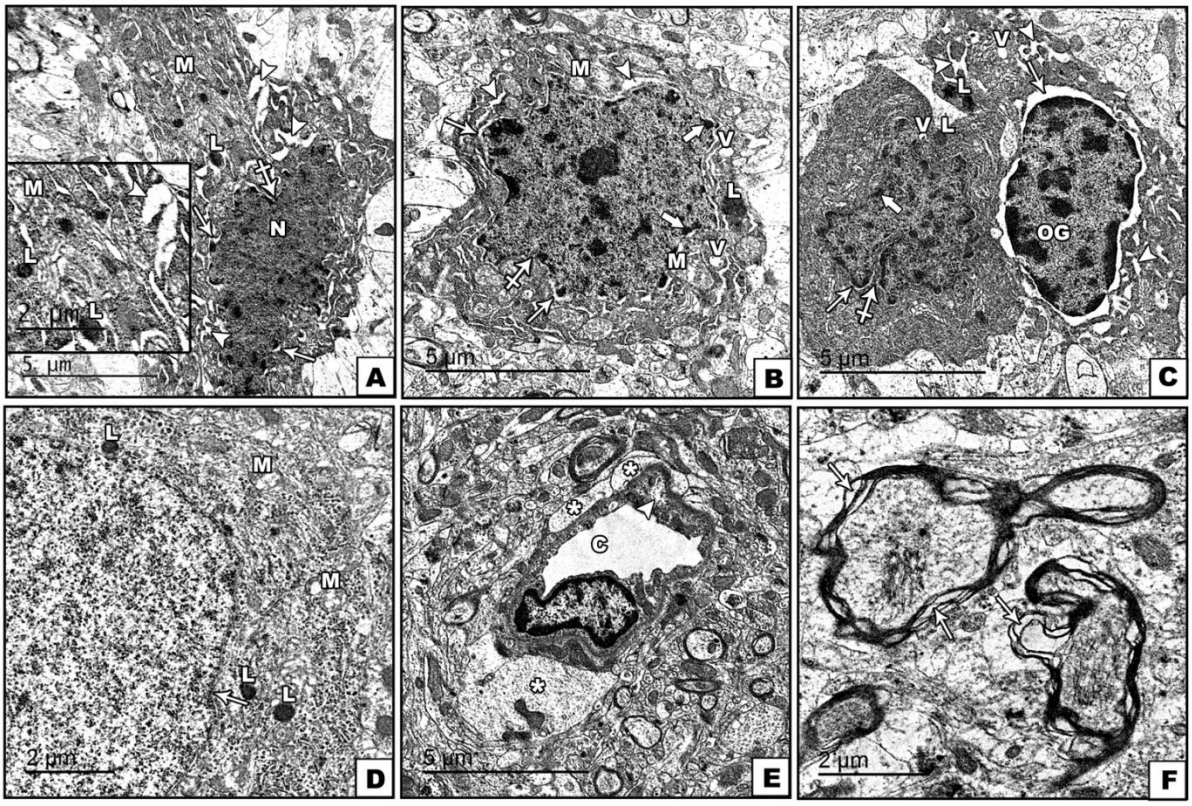

Figure 10: Electron micrographs of Tramadol group motor cortex. (A) showing a shrunken degenerated pyramidal cell with a shrunken dense nucleus (N), wide perinuclear space (arrows) and corrugated nuclear membrane (crossed arrow). Its cytoplasm is dense containing many dilated rER (arrow heads), swollen damaged mitochondria (M) and Lysosomes (L) (Ax 1200, inset: high magnification x2000). (B&C) shrunken pyramidal cells showing wide perinuclear space (arrows), corrugated nuclear membrane (crossed arrows) and chromatin margination (thick arrows). Swollen mitochondria (M) with cristolysis, lysosomes (L) and vacuoles (V) are seen in their cytoplasm. Perineural oligodendrocyte (OG) shows wide perinuclear space (arrow), many dilated rER (arrow heads), lysosomes (L) and vacuoles (V) (B&C x1500). (D) showing a granular cell with invaginated nuclear membrane (arrow), lysosomes (L) and damaged vacuolated mitochondria (M) (x2000). (E) showing a blood capillary (C) with local endothelial cytoplasm swelling (arrow head) and surrounded by enlarged end feet of astrocytes (*) (x1500). (F) irregular arrangement and splitting of myelin lamellae (arrows) is noted in myelinated fibers (x 2500).

PERK immunohistochemically stained sections of the cerebellar cortex of Control and Thyme groups revealed similar pattern of immunostaining. A weak positive PERK immunostaining was observed in few cells of the molecular layer and in few purkinje cells. No statistically significant difference in ID of PERK immunostaining in the layers of cerebellar cortex between the two groups (Figure 7 A, Table 3). In Tramadol group there was a strong positive PERK immunostaining in some cells of molecular layer and all purkinje cells. A moderate positive immunostaining were also observed in some cells and the cerebellar islands of the granular layer (Figure 7B). While, Tramadol+thyme group revealed weak to moderate positive PERK immunostaining in some cells of the molecular layer, in purkinje cells and in cerebellar islands ((Figure 7C). The ID of PERK immunostaining was significantly higher ($p<0.05$) in Tramadol group than Control group. However, it was significantly lower ($p<0.05$) in Tramadol+Thyme group than Tramadol group but remains significantly higher than Control group (Table 3)

Caspase-3 Immunohistochemical staining showed absence of caspase-3 positive cells in the cerebellar cortex of the Control and Thyme groups and there was no statistically significant difference between the two groups in the mean number of caspase-3 positive cells/HPF (Figure 8A, Table 4). Tramadol group revealed many purkinje cells and some cells in the granular layer with strong positive caspase-3 immunoreactivity (Figure 8 B, C). On the other hand, few purkinje cells and few cells in the granular layer showed weak to moderate caspase-3 immunoreactivity in Tramadol+Thyme group (Figure 8 D). A significant increase ($P<0.05$) in the number of caspase-3 positive cells/HPF was found in Tramadol group compared with Control group. While it showed a

significant decrease (P<0.05) in Tramadol+Thyme group compared with Tramadol group but it still showed a significant increase compared with Control group (Table 4).

Ultrastructural findings

Cerebral cortex

Electron microscopic examination of the motor cortex of Control and Thyme groups demonstrated similar ultrastructure. The pyramidal cells had vesicular nuclei with prominent nucleoli and apical dendrites. Their cytoplasm contained Golgi apparatus, Mitochondria, rough endoplasmic reticulum (rER) cisternae and ribosomes (Figure 9 A-C). The granular cells were characterized by rounded highly vesicular nuclei. The cytoplasm showed mitochondria, ribosomes and rER (Figure 9 D, E). The surrounding neuropil revealed neuroglial cells, blood capillaries, nerve fibers and synapses. The oligodendrocyte had heterochromatic nuclei, mitochondria, Golgi, rER and some lysosomes. The blood capillaries were lined with endothelial cells and surrounded by end feets of astrocytes (Figure 9 F, G). The nerve fibers were unmyelinated or myelinated. They contained mitochondria and neurofibrils. Regularly arranged compact myelin lamellae were seen in the myelinated ones (Figure 9 H).

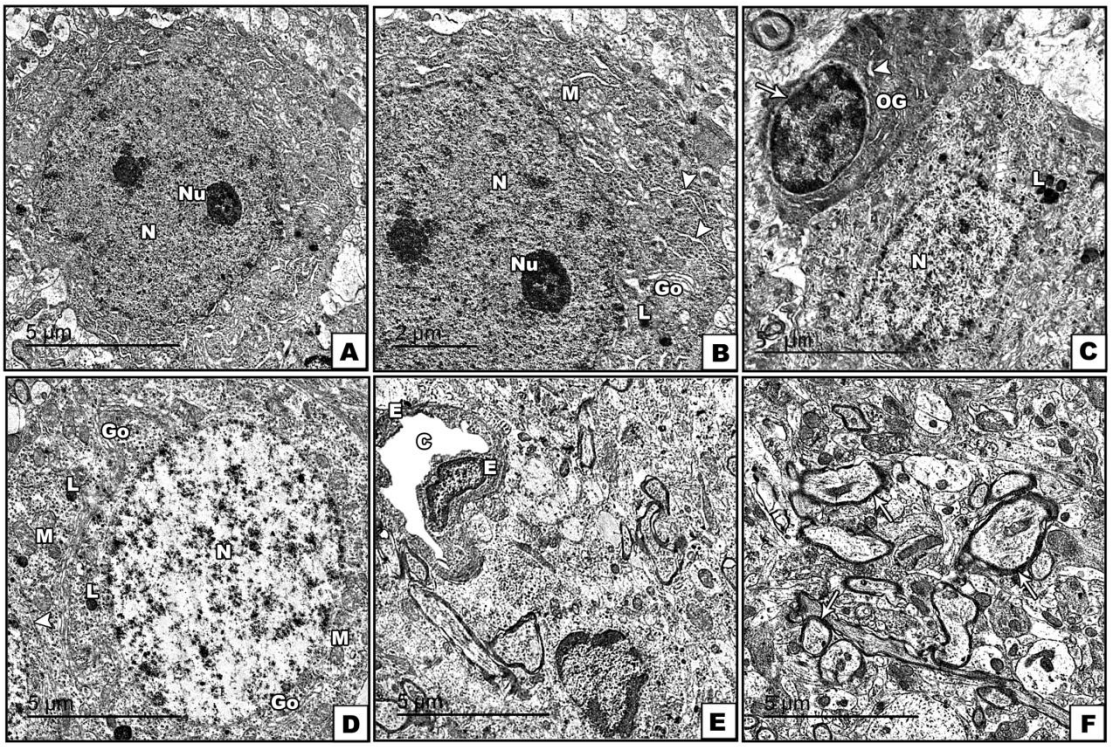

Figure 11: Electron micrographs of motor cortex of Tramadol+Thyme group (A&B) (B: high magnification of A): showing a pyramidal cell with vesicular nucleus (N) and prominent nucleolus (Nu). The cytoplasm revealed rER cisternae (arrow heads), intact mitochondria (M), Golgi saccules (Go) and lysosomes (L) (A x1500, Bx 2000). (C) showing a pyramidal cell with vesicular nucleus (N) and some lysosomes (L). A perineural oligodendrocyte (OG) shows some widening of perinuclear space (arrow) and few dilated rER (arrow head) (x1200). (D) The granular cell demonstrated highly vesicular nucleus (N), intact mitochondria (M), rER (arrow head), Golgi saccules (Go) and lysosomes (L) (x1500). (E) showing blood capillary (C) with intact endothelial cells (E) (x1500). (F) showing regularly arranged compact myelin lamellae (arrows) in the myelinated fibers (x1500).

Obvious ultrastructural changes were detected in Tramadol group motor cortex. Most of the pyramidal cells were shrunken. Their nuclei were dense and shrunhen with wide perinuclear space, corrugated nuclear membrane and chromatin margination. The cytoplasm was dense and showed dilated rER cisternae, swollen mitochondria with damaged cristae, lysosomes and some vacuoles. The Perineural oligodendrocyte also showed wide perinuclear space, many dilated rER, lysosomes and vacuoles (Figure 10 A-C). The granular cells revealed invaginated nuclear membrane damaged vacuolated mitochondria and lysosomes (Figure 10 D). In the neuropil, some blood capillaries showed local endothelial cytoplasm swelling. They are also surrounded by enlarged swollen end feets of astrocytes (Figure 10 E) and many affected myelinated nerve fibers were observed. They showed irregular arrangement and splitting of myelin lamellae (Figure 10 F).

Tramadol+Thyme group showed improved ultrastructure relative to Tramadol group. Most of the pyramidal cells appeared with vesicular nuclei and prominent nucleoli. Their cytoplasm contained intact Golgi, intact rER, mitochondria and some lysosomes (Figure 11 A, B). Perineural oligodendrocyte showed more or less preserved morphology with some widening of the perinuclear space and few dilated rER (Figure 11 C). The granular cells appeared intact and showed highly vesicular nuclei, intact mitochondria, rER, Golgi saccules, ribosomes and some lysosomes (Figure 11 D). The capillaries were lined with intact endothelial cells and no perivascular swelling was observed (Figure 11 E). The majority of myelinated fibers in the neuropil showed regularly arranged compact myelin lamellae (Figure 11 F).

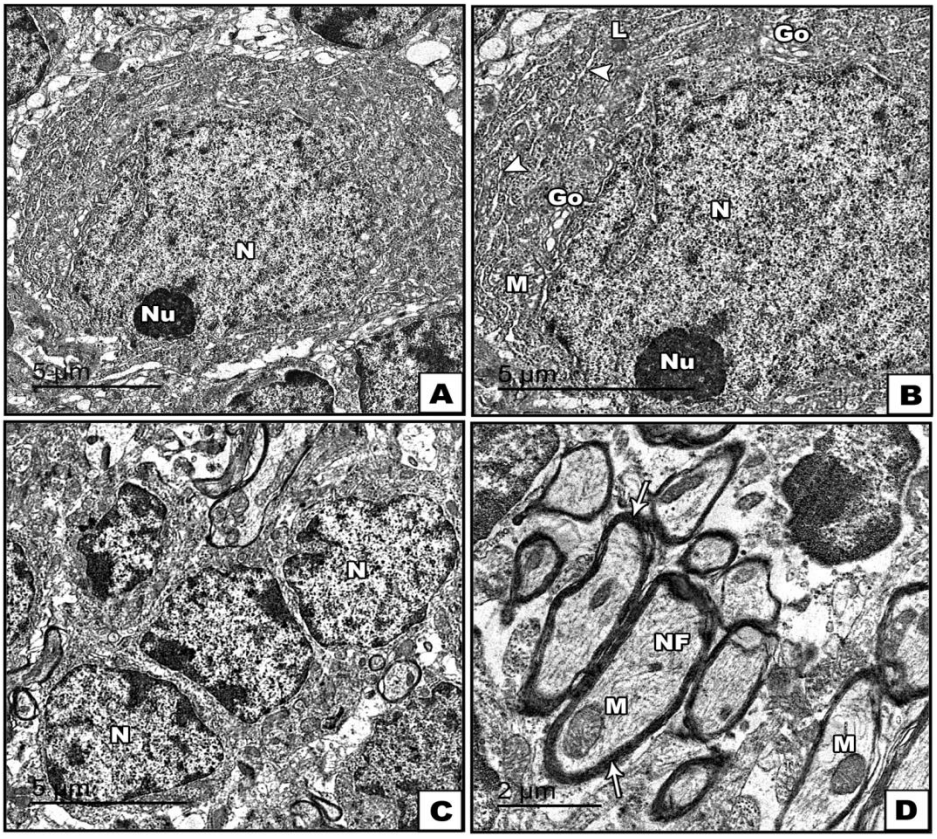

Figure 12: Electron micrographs of the cerebellar cortex of the control group. (A&B) (B: higher magnification of A): showing a purkinje cell with euchromatic nucleus (N) and prominent nucleolus (Nu). The cytoplasm demonstrated mitochondria (M), rER cisternae (arrow heads), Golgi apparatus (Go) and some lysosomes (L) (A x1000, B x1500). (C) showing the granular layer. The granular cells have large nuclei (N) with dense heterochromatin clumps and little cytoplasm containing few organelles (x1200). (D) showing transverse sections in myelinated axons in the granular layer with regular arrangement of myelin lamellae (arrows). The axoplasm contains mitochondria (M) and neurofibrils (NF) (x2000).

Cerebellar cortex

Ultrastructurally, the cerebellar cortex of the Control group showed that purkinje cell had euchromatic nucleus with prominent nucleolus. The cytoplasm revealed mitochondria, rER cisternae, Golgi apparatus and some lysosomes (Figure 12 A, B). The granular cells had large nuclei with dense heterochromatin clumps. Their cytoplasm was little and showed few organelles (Figure 12 C). Myelinated axons were also observed in the granular layer with compact regularly arranged myelin lamellae. Their axoplasm showed mitochondria and neurofibrils (Figure 12 D).

Tramadol group revealed that most of purkinje cells were darkly stained with irregular outlines. The nuclei were darkly stained, irregular and surrounded by wide perinuclear space. Their cytoplasm showed many dilated rER cisternae, numerous secondary lysosomes and damaged mitochondria (Figure 13 A, B). The granular cells had irregular nuclei with more clumps of heterochromatin and surrounded by wide perinuclear spaces (Figure 13 C). Affected myelinated fibers were also noticed and showed splitting and loss of myelin lamellar structure. Mitochondria with damaged cristae were observed in some fibers (Figure 13 D).

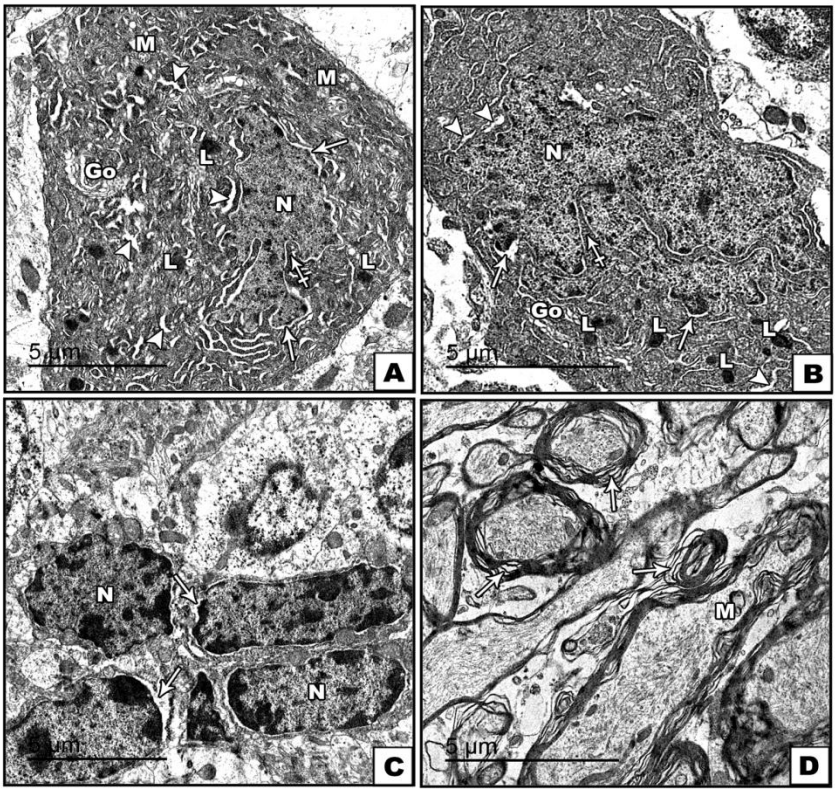

Figure 13: Electron micrographs of the cerebellar cortex of the Tramadol group. (A and B) showing darkly stained purkinje cells with irregular outlines. Their nuclei (N) are irregular (crossed arrows), darkly stained and surrounded by wide perinuclear space (arrows). Many dilated rER cisternae (arrow heads), numerous secondary lysosomes (L), Golgi ssaccules (Go) and damaged swollen mitochondria (M) are observed in their cytoplasm (A x1200, Bx1500). (C) showing the irregular nuclei of the granular (N) cells that surrounded by wide perinuclear space (arrows) and contain more clumps of heterochromatin (x1200). (D) showing myelinated axons with splitting and loss of lamellar structure of myelin (arrows). Some axons contain damaged mitochondria (M) (x1500).

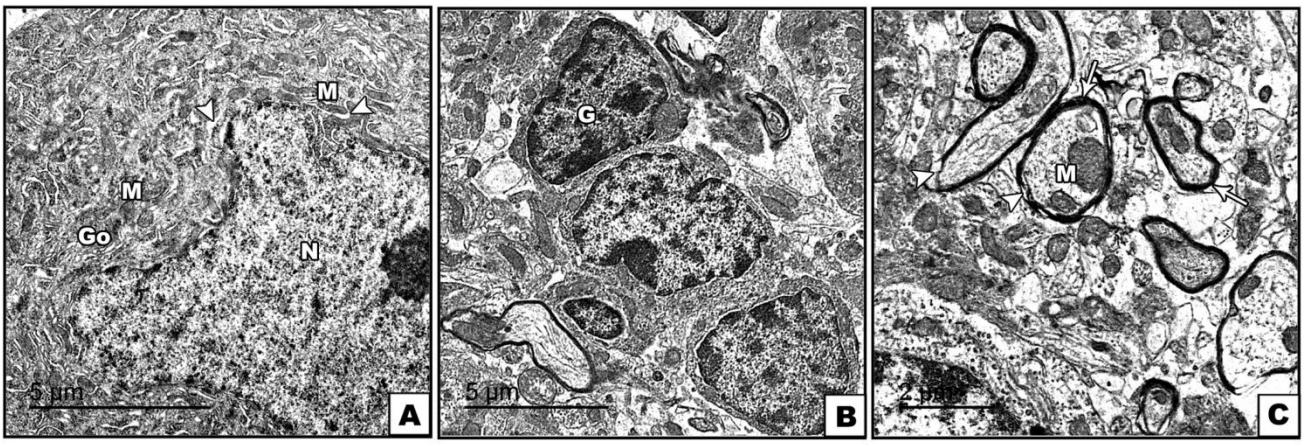

Figure 14: Electron micrographs of the cerebellar cortex of the Tramadol + Thyme group. (A) showing a purkinje cell with euchromatic nucleus (N), Golgi saccules (Go), intact mitochondria (M) and some dilated rER cisternae (arrow heads) (x1500). (B) The granular cells (G) showing nearly intact morphology (x1200). (C) The myelinated axons showing regular compact myelin lamellae (arrows). However, focal areas of myelin splitting are noted (arrow heads). Intact mitochondria (M) are seen in their axoplasm (x2000).

The ultrastructure was improved in Tramadol+Thyme group compared to Tramadol group. Most of the purkinje cells showed euchromatic nuclei, intact mitochondria and Golgi saccules. Some dilated rER cisternae were noted (Figure 14 A). The granular cells had nearly intact morphology (Figure 14 B). Most of the myelinated fibers showed regular compact myelin lamellae. However, focal areas of myelin splitting were found. Intact mitochondria were also seen in the fibers (Figure 14 C).

DISCUSSION

In the current study, Tramadol group revealed marked degenerative and apoptotic changes in the rat motor cerebral and cerebellar cortex. In the motor cortex, the pyramidal neurons were more affected than granular ones. Additionally, neuropil vacuolization was also observed. In the cerebellar cortex, Purkinje cells were markedly damaged and there was vacuolation of cerebellar islands. Our results were similar to that previously reported by many authors in the rat cerebral and cerebellar cortex following chronic tramadol administration.[23-25]

Our described structural changes reflect neuronal damage and different stages of neuronal death. Alongside, it was previously reported that the long term use of opioids causes cell apoptosis with cytoplasmic contraction, reduction in cell volume, chromatin condensation and induces neuronal damage through affection on their cytoskeleton.[26] The observed pericellular halos and spaces in the current study might be due to shrinkage of cells with withdrawal of their processes secondary to cytoskeleton affection. The neuropil and cerebellar islands vacuolization might represent swollen neuronal processes and presynaptic nerve endings.

Among the Tramadol group, the detected dilated congested blood vessels with blood extravasation in the motor cortex might be explained by nitric oxide overproduction by tramadol which has vasodilatory effect.[27] Similarly, dilated cortical vessels with RBCs extravasation and congestion of submeningeal vessels were previously documented following long term intake of tramadol.[23-28]

High oxygen consumption, increased polyunsaturated fatty acids, and low antioxidants level render the brain tissue highly susceptible to oxidative stress.[29] MDA is the most abundant metabolite of free radical-induced lipid peroxidation cascade in biological systems and is commonly used as a marker for oxidative stress.[30] In the present work, significant elevation of MDA level with reduction in SOD and CAT activities in cerebral and cerebellar cortex of Tramadol group relative to Control group indicates that tramadol has a potential induction of oxidative stress. Similarly, tramadol-induced oxidative stress was documented by Ghoneim et al. 2014 in the rat brain tissue where a decrease in gene expression of SOD, CAT and Glutathione peroxidase and an increase in MDA level were found.[31]

Generally, oxidative stress is imbalance between generation of free radicals and cellular antioxidant defenses. ROS are critical signaling molecules that regulate several physiological and pathological conditions. ROS are controlled by antioxidant enzymes including CAT and SOD together with antioxidants which possess scavenging and detoxifying effect.[32,33] ROS are commonly produced in the cytoplasm by mitochondria and ER.[12] Increased ROS levels elicit cell dysfunction through damaging the bio-molecules as protein, lipids and nucleic acids and may lead to cell death through the common apoptotic pathways.[34,35] Hence, tramadol can cause brain tissue injury and apoptosis by ROS generation, lipid peroxidation and decrease of antioxidant defenses and suggested that oxidative stress is an important mechanism in tramadol-caused neurotoxicity.

Multiple intra- and extracellular stimuli can disturb ER function with resultant accumulation of unfolded/misfolded proteins in its lumen leading to ER stress.[12] Excess exogenous ROS is an important stimulus that can disturb protein folding and triggers ER stress; a condition called ROS-dependent ER stress.[36] Under basal conditions, disulfide bond is formed during protein folding with hydrogen peroxide generation which is a major source of ROS.[12] During ER stress, dysregulated cycles of bond formation and breakdown could lead to oxidative stress by ROS accumulation. In addition, Calcium released from the stressed ER enhances mitochondrial ROS production. Both oxidative and ER stress induce each other in a vicious cycle.[10]

ER stress activates UPR pathways to overcome protein folding defects through inhibition of newly formed proteins, transcription of genes coding for proteins needed for folding and degradation of the misfolded proteins. UPR is mediated through three ER stress transmembrane sensors; PERK, IRE1α and ATF6.[4,6] PERK is a protein kinase that belongs to eIF2α kinase subfamily. It consists of cytoplasmic and kinase domains. The cytoplasmic domain senses the accumulation of unfolded/misfolded proteins in ER lumen. PERK is activated by autophosphorylation of its kinase domain. Upon PERK activation, it phosphorylates α-subunit of eukaryotic initiation factor 2 leads to inhibition of protein synthesis.[4,7,37]

In the present study, we observed increased PERK expression in both cerebral and cerebellar cortex of Tramadol group and a significant increase in integrated density of PERK immunostaining compared to Control group. In non-stressed cells, PERK remained inactive by binding of its cytoplasmic domain to Bip/glucose-related protein 78 (BiP/GRP78) in ER lumen. However, during ER stress; BiP/GRP78 is released leading to PERK activation and induction of UPR.[38] This might explain the

increased PERK expression in Tramadol group. These findings together with the observed changes in oxidative stress parameters indicate that tramadol could mediate ER stress and UPR pathways through induction of oxidative stress. In line with our results, activation of ROS-stimulated PERK signaling pathway in a rat model of diabetic cardiomyopathy was reported by Liu et al.[11]

Beside the two classical apoptotic pathways, ER stress is a third major apoptotic pathway.[39] Upon exposure to prolonged ER stress, the UPR fails to rescue the cell and correct the protein folding defects, which initiates the three ER down streaming sensors including PERK. This would lead to apoptosis through many pathways such as caspase-mediated pathway. Several members of Caspases are implicated in ER stress-induced apoptosis. Caspase-12 activates caspase-9, which then activates caspase-3, leading to apoptosis.[7]

In Tramadol group, there was increased caspase-3 expression in both frontal and cerebellar cortex. Besides, significant increase in number of caspase-3 positive cells/HPF was detected. This could highly prove the histologically described degenerative and apoptotic changes in this work. Alongside, the biochemical changes and enhanced PERK expression among this group denote that tramadol could trigger apoptosis through intermingling oxidative and ER stress apoptotic pathways. Concomitantly, a previous study on the effect of tramadol on brain/lung tissues demonstrated an increment in pro-apoptotic Bax and Caspase-3 genes expression.[1]

By electron microscope, the cerebral and cerebellar cortex of tramadol group showed dramatic ultrastructural changes that confirm our histological findings. Degenerated dense shrunken cells with characters of apoptosis such as corrugated nuclear membrane, chromatin margination and abnormal organelles were observed. It has been documented that in early stages of apoptosis, the nuclear membrane becomes invaginated and in late stages the condensed chromatin becomes segregated along the nuclear membrane margins and the cytoplasm shows vacuoles.[40] Similar ultrastructural alterations were observed in the cerebral and cerebellar cortex of tramadol treated rats.[24,25,41]

The observed mitochondrial alterations in this study might be related to oxidative and ER stress. Mitochondria are highly vulnerable to oxidative damage which causes alteration in its permeability and structure.[42,43] In ER-stressed cells, increased Ca^{2+} release from ER opens the mitochondrial permeability transition pores with loss of cytochrome C and activates nitric oxide synthetase leading to ROS production. ROS causes more Ca^{2+} release from ER and creates a vicious cycle that induces mitochondrial dysfunction and induces apoptosis.[12,44] The Dilated rER cisternae might be also due to tramadol-induced lipid peroxidation and ER stress. ER has limited antioxidant defenses which could predispose it to oxidative stress during increased load of protein folding.[45]

Regarding the cytoplasmic vacuoles in the neurons they might be corresponded to swollen mitochondria or due to increased water content in the cells secondary to lipid peroxidation of membranes.[46]

The ultrastructure of oligodendrocytes was altered in Tramadol group, possibly due to oxidative damage. Oligodendrocytes are responsible for myelination in the CNS. In addition, axon abnormalities were found in both cerebral and cerebellar cortex. Myelin abnormalities might be as part of neuronal injury, damage of myelin by free radicals or myelination impairment secondary to damage and dysfunction of oligodendrocytes. Similar alterations were documented in tramadol-induced neurotoxicity and diabetic rat brain.[41,42]

Moreover, some of the cerebral cortical capillaries in Tramadol group demonstrated localized swollen areas in endothelial cytoplasm and enlarged perivascular end-feet of astrocytes. This might be due to lipid peroxidation and increase in cellular water content leading to cell swelling. Consequently, this could induce functional disruption of blood brain barrier.[42]

In this work, the concomitant use of thyme extract and tramadol showed improvement in oxidative stress biochemical parameters compared to Tramadol group. Additionally, improved histological and ultrastructural findings were observed. This was associated with significant decrease in ID of PERK immunostaining and number of caspase-3 positive cells/HPF. These results might be attributed to the antioxidant activity of thyme and indicate its efficient neuroprotective effect against oxidative-stress-mediated tissue injury, ER stress and apoptosis. Its antioxidant effect is owed to its contents of flavonoids, thymol and tetramethoxylated flavones.[15,47] Thyme ability to scavenge free radicals is a major antioxidant mechanism to inhibit lipid peroxidation.[48] It has been mentioned that ER stress and UPR is inhibited by some antioxidants suggesting that induction of ER stress is oxidative stress dependent. This could confirm our observation in decreased PERK expression in this group. Thyme was reported to have neuroprotective effect against hippocampal injury induced by cerebral ischeamia-reperfusion through inhibition of oxidative stress.[49]

CONCLUSION

Tramadol neurotoxicity is strongly thought to be triggered by the complex intermingling of oxidative and ER stresses. PERK; the key ER stress biomarker could be the building bridge that mediates the apoptotic pathway following its activation during ROS-triggered ER stress. Therapeutic targets aimed at enhancing the antioxidant activity, blocking the ROS-mediated ER stress and/or inhibiting the PERK expression pathway may resolve its

neurotoxicity and cell death in tramadol exposed population.

Funding: No funding sources
Conflict of interest: None declared
Ethical approval: The study was approved by the institutional ethics committee, faculty of Medicine, Mansoura University, Egypt

REFERENCES

1. Awadalla EA, Salah-Eldin AE. Molecular and histological changes in cerebral cortex and lung tissues under the effect of tramadol treatment. Biomedicine Pharmacotherapy. 2016;82:269-80.
2. Barbosa J, Faria J, Queirós O, Moreira R, Carvalho F, Dinis-Oliveira RJ. Comparative metabolism of tramadol and tapentadol: a toxicological perspective. Drug Metabolism Rev. 2016;48(4):577-92.
3. Costa I, Oliveira A, Guedes de Pinho P, Teixeira HM, Moreira R, Carvalho F, et al. Postmortem redistribution of tramadol and O-desmethyltramadol. J Analytical Toxicol. 2013;37(9):670-5.
4. Taalab YM, Ibrahim N, Maher A, Hassan M, Mohamed W, Moustafa AA, et al. Mechanisms of disordered neurodegenerative function: concepts and facts about the different roles of the protein kinase RNA-like endoplasmic reticulum kinase (PERK). Reviews Neurosci. 2018.
5. Shen X, Zhang K, Kaufman RJ. The unfolded protein response—a stress signaling pathway of the endoplasmic reticulum. J Chemical Neuroanatomy. 2004;28(1):79-92.
6. Schröder M, Kaufman RJ. ER stress and the unfolded protein response. Mutation Research/Fundamental and Molecular Mechanisms of Mutagenesis. 2005;569(1):29-63.
7. Liu Z, Lv Y, Zhao N, Guan G, Wang J. Protein kinase R-like ER kinase and its role in endoplasmic reticulum stress-decided cell fate. Cell Death Disease. 2015;6(7):e1822.
8. Go BS, Kim J, Yang JH, Choe ES. Psychostimulant-Induced Endoplasmic Reticulum Stress and Neurodegeneration. Molecular Neurobiol. 2016: 1-8.
9. Milisav I, Šuput D, Ribarič S. Unfolded protein response and macroautophagy in Alzheimer's, Parkinson's and prion diseases. Molecules. 2015;20(12):22718-56.
10. Malhotra JD, Kaufman RJ. Endoplasmic reticulum stress and oxidative stress: a vicious cycle or a double-edged sword? Antioxidants & redox signaling. 2007;9(12):2277-94.
11. Liu Z-W, Zhu H-T, Chen K-L, Dong X, Wei J, Qiu C, et al. Protein kinase RNA-like endoplasmic reticulum kinase (PERK) signaling pathway plays a major role in reactive oxygen species (ROS)-mediated endoplasmic reticulum stress-induced apoptosis in diabetic cardiomyopathy. Cardiovascular Diabetol. 2013;12(1):158.
12. Cao SS, Kaufman RJ. Endoplasmic reticulum stress and oxidative stress in cell fate decision and human disease. Antioxidants Redox Signaling. 2014;21(3):396-413.
13. Chong WC, Shastri MD, Eri R. Endoplasmic reticulum stress and oxidative stress: a vicious nexus implicated in bowel disease pathophysiology. International J Molecular Sci. 2017;18(4):771.
14. El-Newary SA, Shaffie NM, Omer E. The protection of Thymus vulgaris leaves alcoholic extract against hepatotoxicity of alcohol in rats. Asian Pacific J Trop Med. 2017;10(4):361-71.
15. Swayeh NH, Abu-Raghif AR, Qasim BJ, Sahib HB. The protective effects of Thymus Vulgaris aqueous extract against Methotrexate-induced hepatic toxicity in rabbits. Int J Pharm Sci Rev Res. 2014;29:187-93.
16. El-Ghawet HA. Effects of tramadol on the reproductive function of wistar albino rats. Eur J Exp Biol. 2015;5:56-64.
17. Ohkawa H, Ohishi N, Yagi K. Assay for lipid peroxides in animal tissues by thiobarbituric acid reaction. Analytical Biochem. 1979;95(2):351-8.
18. Nishikimi M, Rao NA, Yagi K. The occurrence of superoxide anion in the reaction of reduced phenazine methosulfate and molecular oxygen. Biochemical Biophysical Res Communications. 1972;46(2):849-54.
19. Aebi H. Catalase in vitro. Methods in enzymology. 105: Elsevier; 1984: 121-126.
20. Wilson I, Gamble M. Theory and practice of histological techniques. Google Scholar. 2002.
21. Hsu S-M, Raine L, Fanger H. Use of avidin-biotin-peroxidase complex (ABC) in immunoperoxidase techniques: a comparison between ABC and unlabeled antibody (PAP) procedures. J Histochem Cytochem. 1981;29(4):577-80.
22. Bancroft JD, Gamble M. Theory and practice of histological techniques. Elsevier Health Sci; 2008.
23. Omar NM, El-Hawwary AA. The possible ameliorating effect of Nigella sativa oil on tramadol-induced apoptosis in the motor area of rat cerebral cortex: a histological and immunohistochemical study. Egyptian J Histol. 2014;37(1):124-31.
24. Ragab IK, Mohamed HZ. Histological changes of the adult albino rats entorhinal cortex under the effect of tramadol administration: Histological and morphometric study. Alexandria J Med. 2017;53(2):123-33.
25. El-Bermawy MI, Salem MF. Histological changes of the albino rat cerebellar cortex under the effect of different doses of tramadol administration. The Egyptian J Histol. 2015;38(1):143-55.
26. Liu L-W, Lu J, Wang X-H, Fu S-K, Li Q, Lin F-Q. Neuronal apoptosis in morphine addiction and its molecular mechanism. International J Clin Experimental Med. 2013;6(7):540.

27. Ahmed MA, Kurkar A. Effects of opioid (tramadol) treatment on testicular functions in adult male rats: The role of nitric oxide and oxidative stress. Clin Experimental Pharmacol Physiol. 2014;41(4):317-23.
28. Abou El Fatoh M, Farag M, Sayed A, Kamel M, Abdel-Hamid N, Hussein M, et al. Some biochemical, neurochemical, pharmacotoxicological and histopathological alterations induced by long-term administration of tramadol in male rats. Int J Pharm Sci. 2014;4:565-71.
29. Butterfield DA, Castegna A, Lauderback CM, Drake J. Evidence that amyloid beta-peptide-induced lipid peroxidation and its sequelae in Alzheimer's disease brain contribute to neuronal death. Neurobiology Aging. 2002;23(5):655-64.
30. Karaboduk H, Uzunhisarcikli M, Kalender Y. Protective effects of sodium selenite and vitamin e on mercuric chloride-induced cardiotoxicity in male rats. Brazilian Arch Biol Tech. 2015;58(2):229-38.
31. Ghoneim FM, Khalaf HA, Elsamanoudy AZ, Helaly AN. Effect of chronic usage of tramadol on motor cerebral cortex and testicular tissues of adult male albino rats and the effect of its withdrawal: histological, immunohistochemical and biochemical study. Int J Clin Exp Pathol. 2014;7(11):7323.
32. Circu ML, Aw TY. Reactive oxygen species, cellular redox systems, and apoptosis. Free Radical Biol Med. 2010;48(6):749-62.
33. Fulda S, Gorman AM, Hori O, Samali A. Cellular stress responses: cell survival and cell death. Int J Cell Biol. 2010;2010.
34. Ott M, Gogvadze V, Orrenius S, Zhivotovsky B. Mitochondria, oxidative stress and cell death. Apoptosis. 2007;12(5):913-22.
35. Ryter SW, Kim HP, Hoetzel A, Park JW, Nakahira K, Wang X, et al. Mechanisms of cell death in oxidative stress. Antioxidants Redox Signaling. 2007;9(1):49-89.
36. Ding W, Yang L, Zhang M, Gu Y. Reactive oxygen species-mediated endoplasmic reticulum stress contributes to aldosterone-induced apoptosis in tubular epithelial cells. Biochem Biophysical Res Communications. 2012;418(3):451-6.
37. Saito A, Ochiai K, Kondo S, Tsumagari K, Murakami T, Cavener DR, et al. Endoplasmic reticulum stress response mediated by the PERK-eIF2α-ATF4 pathway is involved in osteoblast differentiation induced by BMP2. J Biol Chem. 2011;286(6):4809-18.
38. Gardner BM, Walter P. Unfolded proteins are Ire1-activating ligands that directly induce the unfolded protein response. Science. 2011;333(6051):1891-4.
39. Szegezdi E, Logue SE, Gorman AM, Samali A. Mediators of endoplasmic reticulum stress-induced apoptosis. EMBO reports. 2006;7(9):880-5.
40. Tiso M, Gangemi R, Severi AB, Pizzolitto S, Fabbi M, Risso A. Spontaneous apoptosis in human thymocytes. Am J Pathol. 1995;147(2):434.
41. Omar NM. Nigella sativa oil alleviates ultrastructural alterations induced by tramadol in rat motor cerebral cortex. J Microscopy Ultrastructure. 2016;4(2):76-84.
42. Hernández-Fonseca JP, Rincón J, Pedreañez A, Viera N, Arcaya JL, Carrizo E, et al. Structural and ultrastructural analysis of cerebral cortex, cerebellum, and hypothalamus from diabetic rats. Experimental Diabetes Res. 2009;2009.
43. Guo C, Sun L, Chen X, Zhang D. Oxidative stress, mitochondrial damage and neurodegenerative diseases. Neural Regeneration Res. 2013;8(21):2003.
44. Brand MD. The sites and topology of mitochondrial superoxide production. Experimental Gerontol. 2010;45(7-8):466-72.
45. Santos CX, Tanaka LY, Wosniak Jr J, Laurindo FR. Mechanisms and implications of reactive oxygen species generation during the unfolded protein response: roles of endoplasmic reticulum oxidoreductases, mitochondrial electron transport, and NADPH oxidase. Antioxidants Redox Signaling. 2009;11(10):2409-27.
46. Afifi OK, Embaby AS. Histological study on the protective role of ascorbic acid on cadmium induced cerebral cortical neurotoxicity in adult male albino rats. J Microscopy Ultrastructure. 2016;4(1):36-45.
47. Jafarisani M, Masoomikarimi M, Kazemi SS, Mirzaeidelaviz S, Naderi Z, Ahmadi R. Effect of Thymus Vulgaris Ethanol Extract, on Serum Total Antioxidant in Experimental Induced Poly Cystic Ovarian Syndrome (PCOs) Rats. Int J Health Studies. 2016;2(1):30-4.
48. Lee S-J, Umano K, Shibamoto T, Lee K-G. Identification of volatile components in basil (Ocimum basilicum L.) and thyme leaves (Thymus vulgaris L.) and their antioxidant properties. Food Chemistry. 2005;91(1):131-7.
49. Setorki M, Mirzapoor S. Evaluation of Thymus vulgaris Extract on Hippocampal Injury Induced by Transient Global Cerebral Ischemia and Reperfusion in Rat. Zahedan J Res Med Sci. 2017;19(5):e9216.

Cite this article as: Sarhan NR, Taalab YM. Oxidative stress/PERK/ apoptotic pathways interaction contribute to tramadol neurotoxicity in rat cerebral and cerebellar cortex and thyme enhances the antioxidant defense system: histological, immunohistochemical and ultrastructural study. Int J Sci Rep 2018;4(6):124-41.